Supporting Information

Cu-BTC-confined synthesis of Cu-Cu$_2$O-CuS nanojunctions embedded in a porous carbon matrix for remarkable photothermal CO$_2$ conversion

Yajie Chen, Yi Ding, Wei Han, Wei Li, Xinyan Yu, Guohui Tian*

Key Laboratory of Functional Inorganic Material Chemistry, Ministry of Education of

the People's Republic of China, Heilongjiang University, Harbin 150080 P. R. China.

E-mail: tiangh@hlju.edu.cn

Table of Contents

Experimental Section/Methods

Supplementary Fig.s and table

Experimental Section/Methods

Sample characterization: The crystal structure, microstructure, and morphology of the samples were analyzed by an X-ray diffractometer (XRD, Rigaku, SmartLab 9 KW), transmission electron microscopy (TEM, JEOL, JEM-F200) and scanning electron microscopy (SEM, ZEISS, SIGMA 500). X-ray photoelectron spectroscopy (XPS) tests were finished on Kratos-AXISULTRA DLD, and Al Kα is the X-ray source. UV-vis diffuse reflectance spectra (DSR) were obtained from an UV-Vis spectrophotometer (Lambda 750, Perkin Elmer). The photoluminescence (PL) spectra were recorded from a fluorescence spectrophotometer (F-7000, Hitachi). N_2 adsorption-desorption and CO_2 adsorption isotherms were acquired on a Micrometritic analyzer (ASAP 2040, Micromeritics) at 77 and 273.15 K, respectively. In situ diffuse reflectance Fourier transform spectra (DRIFTS) were achieved from Nicolet IS-50 infrared spectrometer. CO_2 temperature-programmed desorption (CO_2-TPD) tests were finished on a ChemBET Pulsar Quantachrome.

Photoelectrochemical measurements: The photoelectrochemical tests were finished on a CHI760e electrochemical system with a working electrode, a Pt wire as the counter electrode, and an Ag/AgCl electrode as the reference electrode. Electrolyte is 0.5 M Na_2SO_4. The Xe lamp (300 W) with a filter was applied, and the light illumination range is Vis-NIR light (400 nm $\leq \lambda \leq$ 1100 nm). The Mott-Schottky curves were acquired with various frequencies (0.5, 1, and 1.5 kHz) under dark conditions. The electrochemical impedance spectra (EIS) were measured over $0.1\text{-}10^5$ Hz at an amplitude of 5 mV.

The details of oxygen detection

The air residuals (N_2+O_2) was tested before light irradiation in each experiment. The O_2 generation was obtained by subtracting the air residuals. The theoretical of O_2 formation was calculated by (O_2 formation rate) = [(CO formation rate)/2+(CH_4 formation rate)×2].

Calculation of Apparent Quantum Yield (QE %):

The apparent quantum yield (QE) is defined as the ratio of number of reacted electrons to the number of incident photons. In general, two electrons are required to produce one CO molecule, whereas, eight electrons are needed to produce one CH_4 molecule. The apparent quantum yield (QE) measurement was performed using the equation below:

$$QE\ (\%) = \frac{2 \times N_a \times N_{(CO)} + 8 \times N_a \times N_{(CH_4)}}{I \times A \times \dfrac{\lambda}{hc} \times t} \times 100\%$$

where, $N_{(CO)}$ is number of CO (mole) evolved and $N_{(CH4)}$ is number of CH_4 (mole) evolved in time "t" (1 h), N_a is Avogadro's number ($N = 6.022 \times 10^{23}$ mol^{-1}), I is the incident solar irradiance ($I = 1.5$ mW cm^{-2}), LED (5 W, Beijing Perfectlight Technology Co. Ltd., China) was positioned 4.0 cm above the reactor, and the focused areas in the reactor for LED was 4 cm^{-2}. λ is the wavelength of the present study (420 and 550 nm), h is Planck's constant (6.62×10^{-34} J·s), c is the speed of light (3.0×10^8 m s^{-1}).
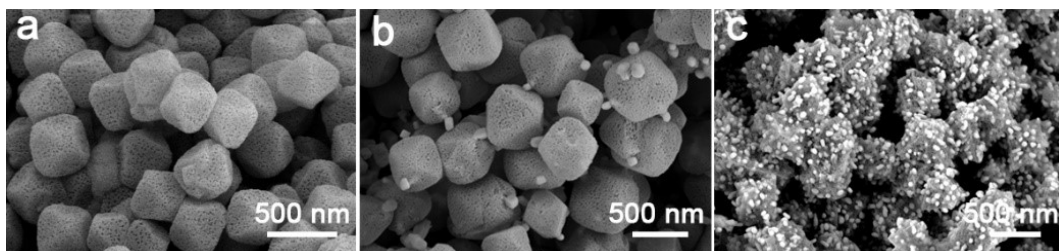
Supplementary Fig.s and Tables

Fig. S1. SEM images of Cu-Cu$_2$O@C obtained different thermal oxidation time. (a) 10 min, (b) 45 min, and 60 min.
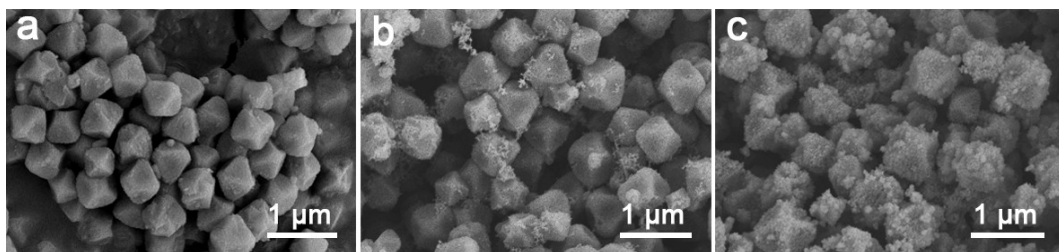

Fig. S2. SEM images images of Cu-Cu$_2$O-CuS@C samples prepared from different sulfidation time. (a) 10 min, (b) 45 min, and 60 min.
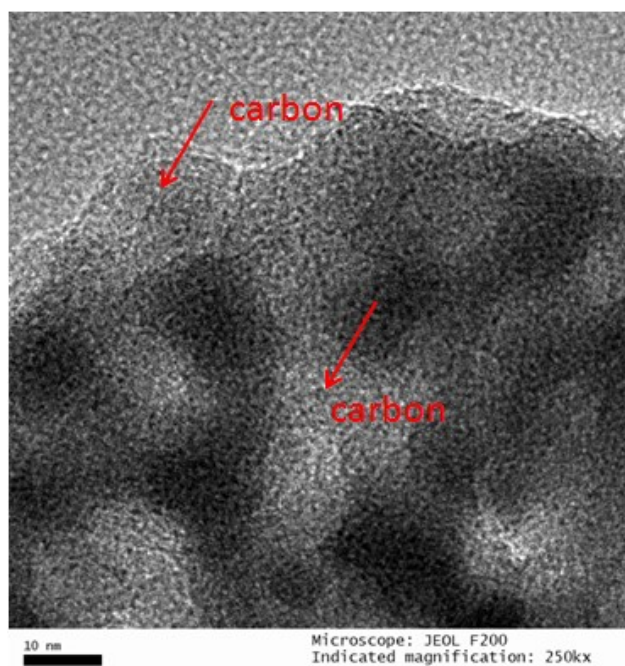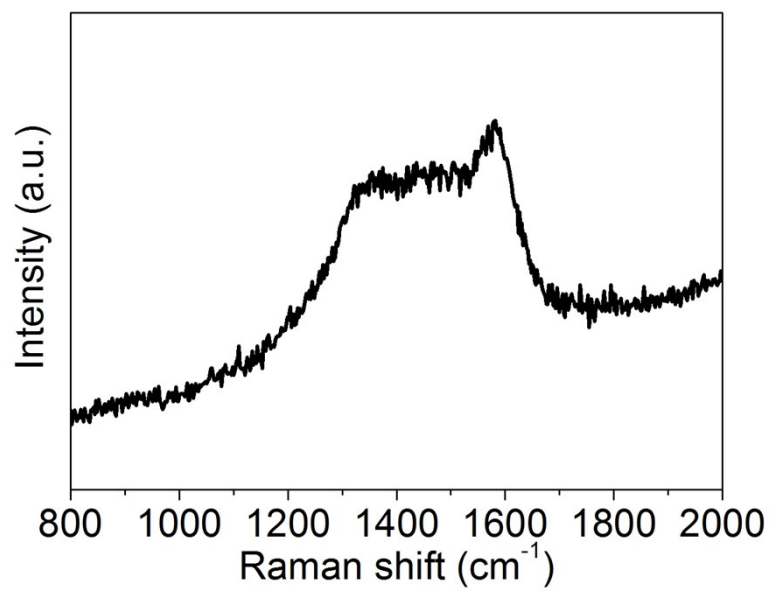
Fig. S3. High magnification TEM image of Cu@C.

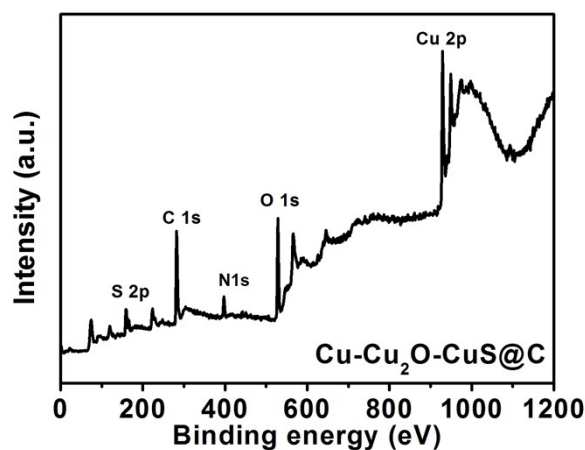
Fig. S4. Raman spectrum of Cu@C.

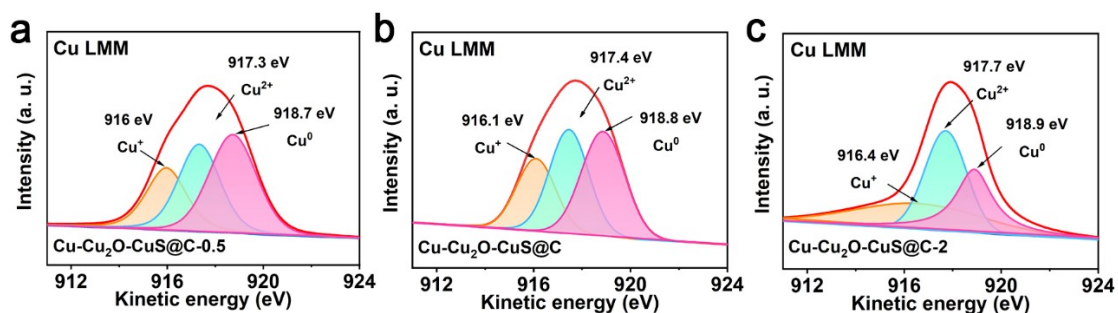**Fig. S5.** Survey XPS spectrum of Cu-Cu$_2$O-CuS@C.

Fig. S6. Auger spectra of Cu-Cu$_2$O-CuS@C-0.5 (a), Cu-Cu$_2$O-CuS@C (b), and Cu-Cu$_2$O-CuS@C-2 (c).

Table S1. Summary of the Cu LMM peak-fitting results

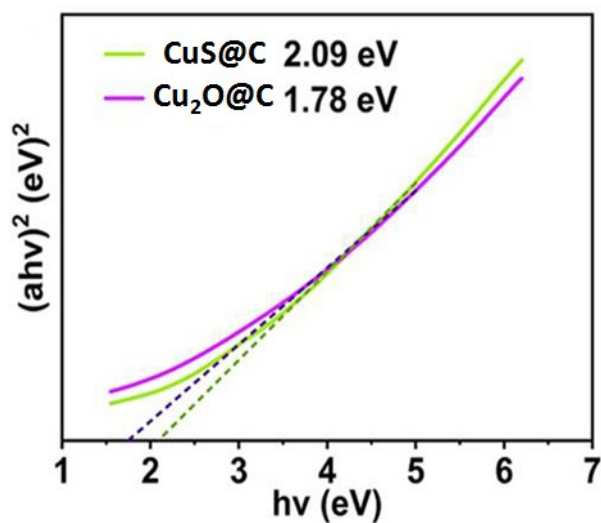| Sample	Cu-Cu$_2$O-CuS@C-0.5		Cu-Cu$_2$O-CuS@C		Cu-Cu$_2$O-CuS@C-2	
	K.E.(eV)	At.%	K.E.(eV)	At.%	K.E.(eV)	At.%
Cu^o	918.7	42.3	918.8	39.6	918.9	30.7
Cu$^+$	916.0	23.8	916.1	23.5	916.4	23.1
Cu^{2+}	917.3	33.9	917.4	36.9	917.7	46.2
Cu^0:Cu$^+$:Cu^{2+}		10:5:8		8:4:7		7:2:13

Fig. S7. The Tauc plots of the samples derived from the UV-Vis diffuse reflectance spectra in Fig. 6d.
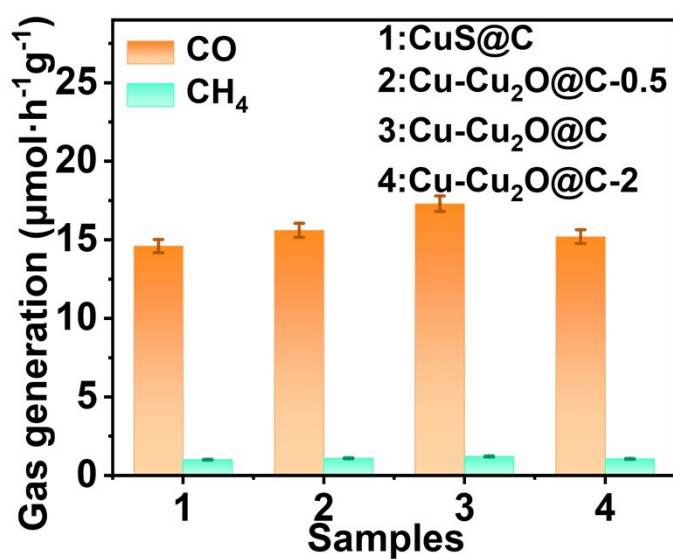

Fig. S8. Time-yield plots of CO (a) and CH_4 (b) generated from photocatalytic CO_2 reduction over Cu-Cu$_2$O@C samples (Cu-Cu$_2$O@C-0.5, Cu-Cu$_2$O@C, Cu-Cu$_2$O@C-2, and Cu$_2$O@C) with different Cu/Cu$_2$O ratios under Vis-NIR light irradiation. (based on 3 separate measurements, error estimates: 3.03 %).
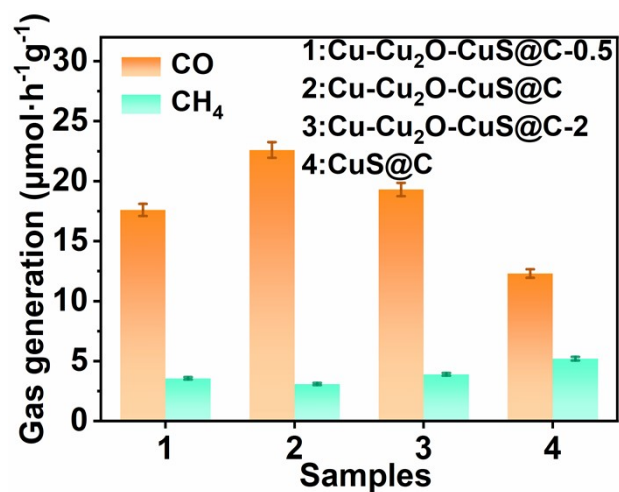
Fig. S9. Average yields of CO (a) and CH_4 (b) generated from photocatalytic CO_2 reduction over the $Cu-Cu_2O-CuS@C$ samples with different sulfidation degree. (based on 3 separate measurements, error estimates: 3.01 %).
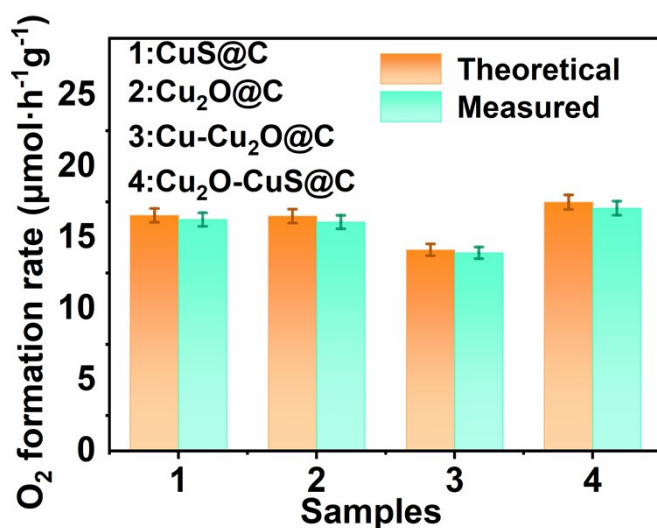

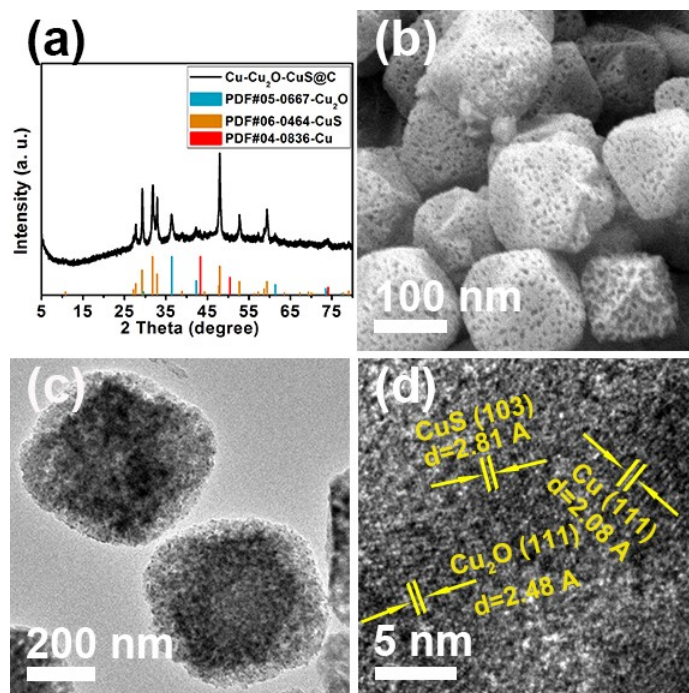**Fig. S10.** The O_2 formation rate of different photocatalysts. (based on 3 separate measurements, error estimates: 3.08 %).

.

Fig. S11. (a) XRD pattern, (b) SEM, (c) TEM, and (d) HRTEM images of Cu-Cu_2O-CuS@C after CO_2 reduction reaction tests.
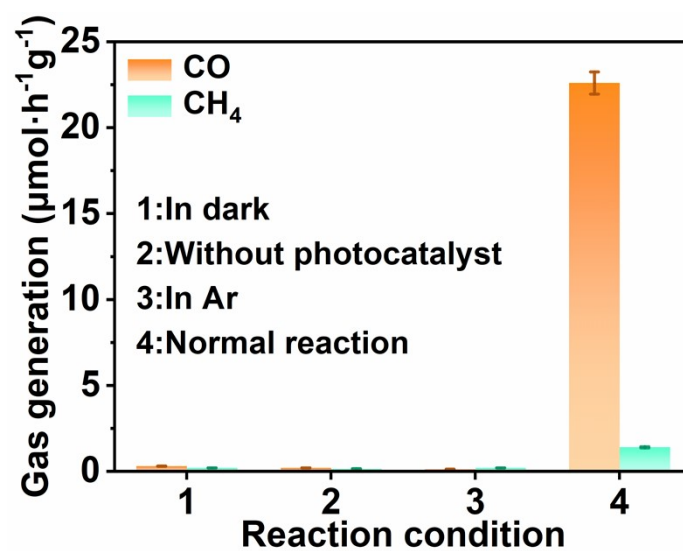

Fig. S12. Average production rates of CO and CH_4 over Cu-Cu_2O-CuS@C samples under different photocatalytic conditions. (based on 3 separate measurements, error estimates: 2.97 %).
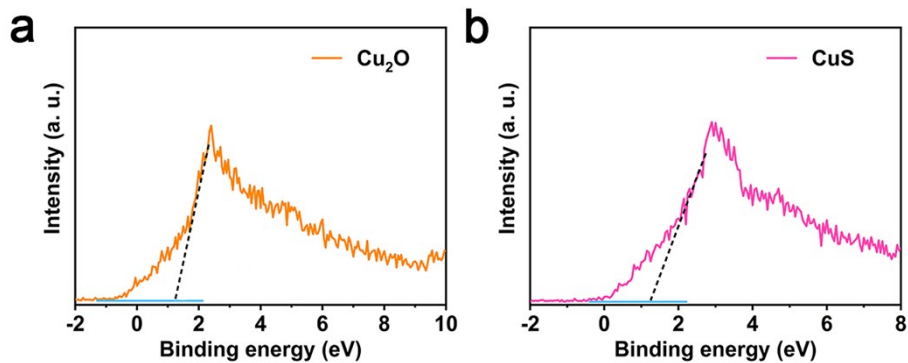
Fig. S13. XPS valence band spectra of (a) Cu_2O and (b) CuS.
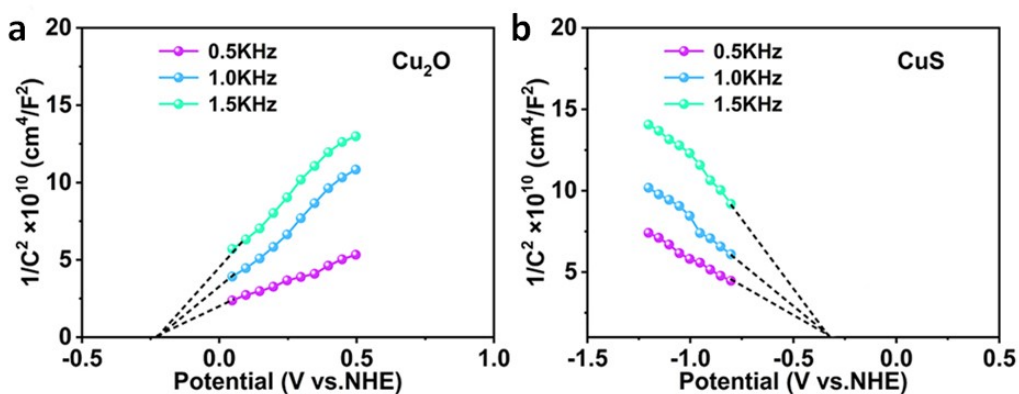
Fig. S14. Mott-Schottky plots of (a) Cu_2O and (b) CuS.

Table S2. The surface area (S_{BET}), pore volume and average pore size of the samples were prepared.

Samples	S_{BET} (m^2 g^{-1})	Pore volume (cm^3 g^{-1})	Average pore size (nm)
Cu-BTC	706.5	0.31	0.5
Cu_2O@C	40.1	0.11	12.3
Cu-Cu_2O@C	60.8	0.22	17.1
Cu-Cu_2O-CuS@C	83.4	0.33	19.4
CuS@C	43.9	0.14	13.1

Table S3. The summary of CO and CH_4 productions from the photocatalytic conversion of CO_2 over different samples under Vis-NIR light irradiation. (experiment times: 3, error estimates: 2.95 %).

Photocatalyst	CO yield (μmol g^{-1}h^{-1})	CH$_4$ yield (μmol g^{-1}h^{-1})	CO selectivity (%)	QE (%), λ=420 nm	QE (%), λ=550 nm
CuS@C	12.2±0.3	5.10±0.1	37.4±1.0	0.706±0.02	0.568±0.01
Cu$_2$O@C	14.5±0.4	4.50±0.1	44.6±1.2	0.958±0.02	0.636±0.01
Cu-Cu$_2$O-CuS@C	22.5±0.6	3.08±0.1	64.6±1.8	1.926±0.05	1.586±0.04
Cu-Cu$_2$O@C	17.2±0.4	2.73±0.1	61.1±1.7	1.403±0.04	1.081±0.03

Table S4. Summary of the photoluminescence decay time (τ) and their relative intensities of different samples.

Sample	τ_1 (ns)	τ_2 (ns)	B_1	B_2	Average lifetime (τ, ns)
Cu-Cu$_2$O@C	1.8	14.1	62.1	37.9	13.8 ± 0.3
Cu$_2$O@C	1.5	10.1	65.6	34.4	8.2 ± 0.3
Cu-Cu$_2$O-CuS@C	2.6	17.6	51.9	48.1	15.5 ± 0.4
CuS@C	1.1	8.9	68.3	31.7	7.1± 0.2

The average lifetime was calculated using the equation: $(\tau)=(B_1\tau_1^2+ B_2\tau_2^2)/(B_1\tau_1+ B_2\tau_2)$. (experiment times: 3, error estimates: 2.92%).

Table S5. Fitting results for Nyquist plots of the different samples.

Sample	$R_s(\Omega)$	$R_{ct}(\Omega)$	$C_{ct}(\mu F)$
CuS@C	11.56	23.34	0.329
Cu$_2$O@C	9.42	19.19	0.422
Cu-Cu$_2$O@C	8.90	17.63	0.432
Cu-Cu$_2$O-CuS@C	7.12	15.12	0.478

Table S6. The energy band parameters of the samples.

Sample	E_g (eV)	E_f (eV)	XPS VB (eV)	E_{VBT} (eV)	E_{CBB} (eV)
CuS	2.09	-0.35	1.18	0.73	-1.36
Cu$_2$O	1.78	-0.24	1.17	0.93	-0.86